The Appearance of Rapidly Flowing Blood on Magnetic Resonance Images

William G. Bradley, Jr.[1]
Victor Waluch[1]
Ka-Siu Lai[1]
Erik J. Fernandez[2]
Clara Spalter[2]

The appearance of rapidly flowing blood on imaging (MRI) was evaluated using flow phantoms and dye infusion experiments. Laminar flow can be maintained at high velocities in small-diameter vessels. Under such conditions, flow-related enhancement may be observed several slices into a multislice imaging volume. Decreasing cross-sectional area of the unsaturated protons in the midstream is noted on slices further removed from the entry surface. As the velocity increases, turbulence occurs. The increased random motion of the protons causes loss of intensity on the first-echo image, although rephasing with increased intensity can be noted on the second-echo image. The flow pattern of a simple intraluminal obstruction is demonstrated by MRI and dye infusion experiments. Rephasing is noted within the eddy downstream from the obstruction. Clinical examples of the phantom findings are shown and applications are discussed.

The appearance of flowing blood on magnetic resonance images (MRI) has been the subject of several reports [1–9]. Hawkes et al. [1] first demonstrated loss of signal from an arteriovenous malformation in the brain. This was alledgedly due to blood flowing through the selective slice too rapidly to return a spin-echo signal. Young et al. [2] showed increased signal in the rapidly flowing carotid arteries using a saturation-recovery (repeated free induction decay) pulsing sequence. Similar increased intensity has been noted for slowly flowing blood and has been called "paradoxical enhancement" [4]. Paradoxical enhancement was subsequently divided into two phenomena [9]: "flow-related enhancement" and "even-echo rephasing." Flow-related enhancement is present when saturated, fully magnetized protons first enter the imaging volume, giving a stronger intraluminal signal than that from partially saturated protons in the adjacent stationary tissue. Even-echo rephasing refers to the increased intraluminal signal present on even-echo images relative to their odd-echo counterparts in a multiecho pulsing sequence [7]. For flow into a slice-selecting gradient field, rephasing occurs after each 360° of rotation after the initial 90° pulse (i.e., for all even echoes).

The MRI appearance of turbulence has been a matter of some debate in the literature. Mills et al. [8] state, "The effect of turbulence is to maintain a subpopulation of protons within the imaged plane and, thus, *increase* [italics added] the signal." On the other hand, Bradley and Waluch [9] have stated that the increased random motion associated with turbulence should lead to additional loss of coherence with subsequent *decrease* in signal intensity.

Our study was undertaken to evaluate the appearance of rapidly flowing blood. Both rapid laminar flow and turbulent flow were considered. The MRI appearance is correlated with theoretical predictions of turbulence as well as with demonstrated turbulence using dye-injection experiments.

"High velocity" and "turbulence" are not equivalent terms. Laminar flow can be maintained at high velocity in small-diameter tubes. On the other hand, turbulence occurs at lower velocities in larger-diameter tubes. Turbulence is present [10] when

Received June 29, 1984; accepted after revision September 7, 1984.

Presented at the annual meeting of the American Roentgen Ray Society, Las Vegas, April 1984.

V. Waluch is a Diasonics MR Fellow.

[1] NMR Imaging Laboratory, Huntington Medical Research Institutes, 18 Pico St., Pasadena, CA 91105. Address reprint requests to W. G. Bradley, Jr.

[2] Department of Chemical Engineering, California Institute of Technology, Pasadena, CA 91105.

AJR 143:1167–1174, December 1984
0361–803X/84/1436–1167

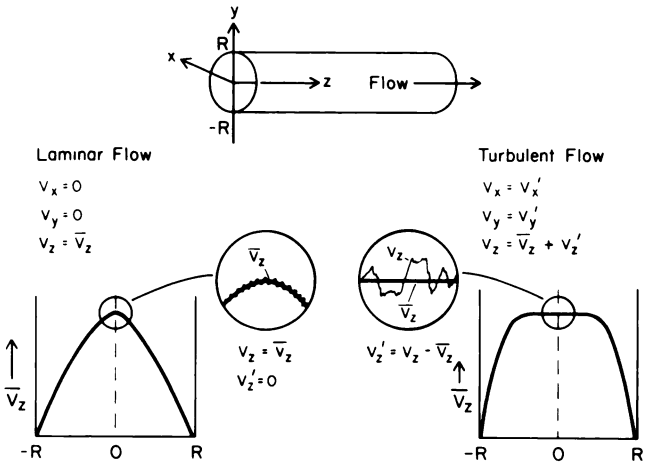

Fig. 1.—Comparison of laminar and turbulent flow. For flow in tube of radius R in axial (z) direction, velocity components in nonaxial direction (V_x and V_y) are zero during laminar flow. Actual velocity in axial direction (V_z) is equal to time-smoothed mean ($\bar{V}_z$). In turbulent flow, fluctuating velocity components are present (indicated by superscript primes, e.g., v_x').

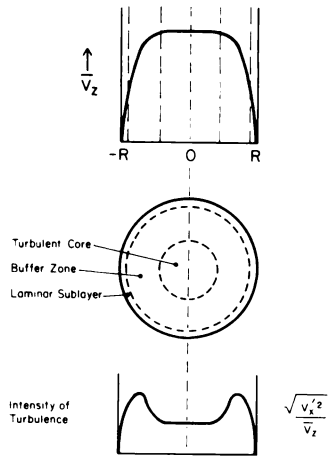

Fig. 2.—Transitional flow in tube of radius R. **Top,** Lateral view: flattened flow profile of time-smooth mean velocity ($\bar{V}_z$) is shown. **Middle,** Axial view: turbulent core, buffer zone, and laminar sublayer are demonstrated. **Bottom,** Lateral projection: intensity of turbulence is plotted as function of radial position. Magnitude of fluctuating velocity component, $\sqrt{V_x'^2}/\bar{V}_z$ (i.e., intensity of turbulence), is greatest in buffer zone.

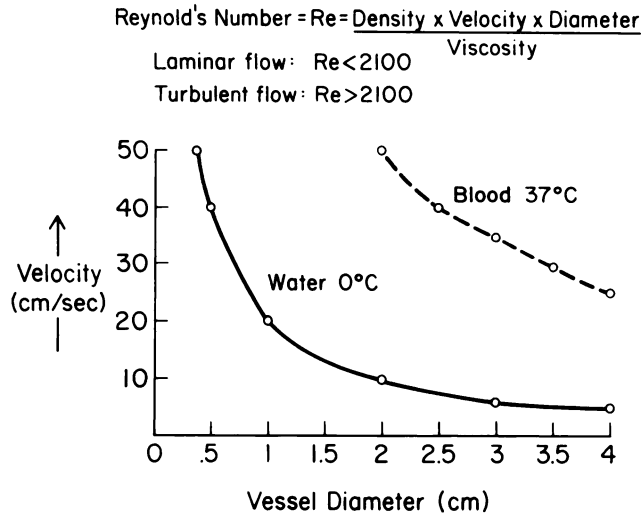

Fig. 3.—Reynolds number (Re) prediction of turbulence. Re (dimensionless) = [density (g/cm^3) × average velocity (cm/sec) × tube diameter (cm)]/viscosity (centipoise = 0.01 g/cm-sec). Reynolds relationship is shown and velocity of onset of turbulence plotted for different vascular diameters for blood and water. Notice that turbulence occurs at lower velocities in larger-diameter vessels and that blood, with its greatest viscosity, can maintain laminar flow at higher velocities than water.

fluctuating velocity components are found in both the axial and nonaxial directions (fig. 1). The velocity profile is flatter for turbulent or "plug" flow than for laminar flow, where the velocity profile is parabolic. Several regions can be defined [10] for flow rates in transition between laminar flow and turbulent flow in a tube (fig. 2). Fully developed turbulence is present in the core. Laminar flow is present in a thin sublayer at the boundary of the tube. In between, there is a buffer zone separating the turbulent core from the laminar sublayer. Curiously, the magnitude of the random fluctuating velocity components (i.e., the intensity of turbulence) is greatest in the buffer zone [10].

As an approximation, onset of turbulence can be predicted using the Reynolds number Re, which is defined [10, 11]: Re = (density × velocity × tube diameter)/viscosity. For Reynolds numbers less than 2100, laminar flow is generally present; for Reynolds numbers greater than 2100, turbulent flow is present. The lowest velocity at which turbulence occurs is plotted as a function of vessel diameter in figure 3 for water and blood. It should be emphasized that this is a gross approximation, only applying to steady flow in smooth-walled tubes without branch points [10, 11].

High-velocity signal loss (fig. 4) occurs when protons do not remain within the selected slice long enough to acquire both the initial 90° pulse and a 180° pulse to produce a spin echo. More signal is lost for later echoes because the protons do not remain within the slice for the longer time interval between the initial 90° pulse and the 180° pulse preceding the last echo. The degree of high-velocity signal loss is a linear function of velocity that remain within the slice for the appropriate radiofrequency (RF) pulses and those that do not. The latter can be further divided into protons that flow *into* the upstream side of the slice (not having acquired the initial 90° pulse) and those that flow *out of* the slice before acquiring the 180° pulse. If we follow the course of all protons that were in the slice at the time of the initial 90° pulse, each will have moved a distance $v \cdot TE/2$ during the interpulse interval TE/2. Those protons moving a distance equal to one slice thickness Δz or more will return no signal. The fraction of protons flowing out of the volume is therefore: $(v \cdot TE/2)/\Delta z$. The fraction of protons remaining within the volume is then: $1 - [(v \cdot TE/2)/\Delta z]$. Since the MR signal is proportional to the number of protons that remain within the slice, it should also be proportional to this ratio. In figure 5, theoretical MR intensity is plotted as a function of velocity (for tubes less than 0.4 cm in diameter so that laminar flow is present even at the highest flow rates).

Increased intraluminal signal due to even-echo rephasing

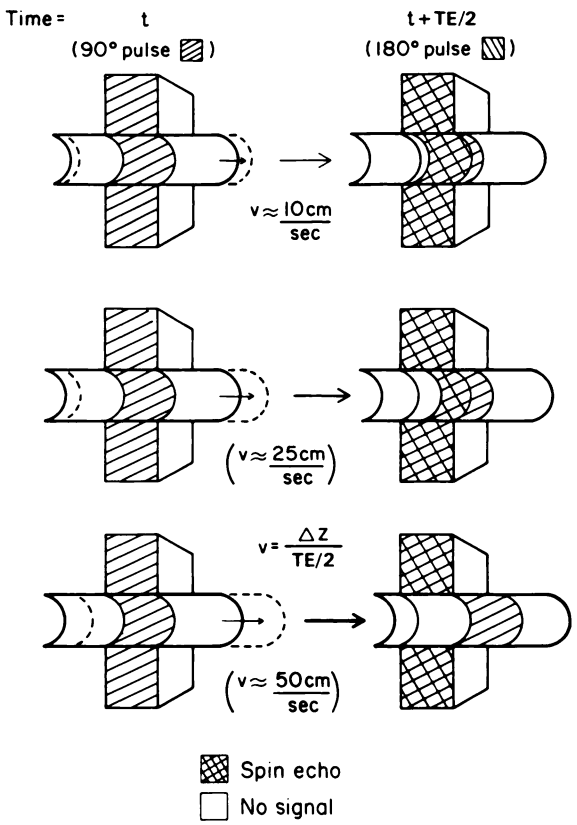

Fig. 4.—High-velocity signal loss. Signal is lost from protons that are not within slice at time of both 90° and 180° selective pulses. Total signal loss occurs when velocity is such that distance of one slice thickness ΔZ is traversed during interpulse interval TE/2.

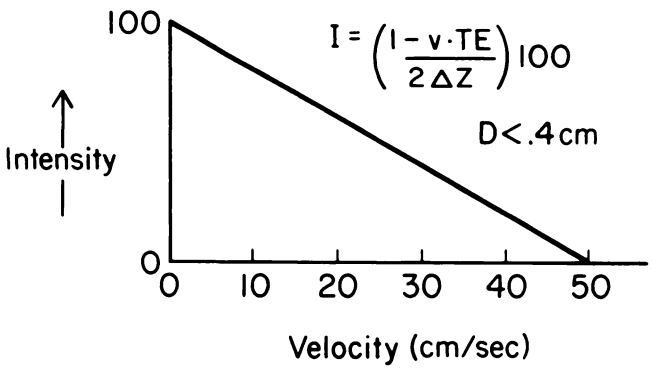

Fig. 5.—High-velocity signal loss. Predicted intraluminal intensity (I) is plotted as function of velocity v for tubes less than 0.4 cm in diameter (D). This illustrates linear relation predicted between signal intensity and velocity, modified by slice thickness Δz and echo-delay time TE.

has been described previously for slow laminar flow [7]. Even-echo rephasing has also been demonstrated during turbulent flow [12, 13], although this has not previously been described in the MRI literature. Relatively increased signal has been demonstrated from the even echoes in a multiecho sequence [13]. This can be predicted theoretically if one assumes a gaussian distribution of the random fluctuating velocity components about the time-smoothed mean [12]. In addition to high velocity, turbulence can be caused by luminal obstruction where large-scale recirculation zones (eddies) are formed. Rephasing would then be expected within the laminar flow regime of the eddy.

The appearance of rapid blood flow on MRI was considered in light of the above theoretical considerations and examined using flow phantoms and dye-infusion experiments. The potential application of these findings to clinical situations is considered.

Materials and Methods

MRI was performed on a commercially available Diasonics 0.35-T MR imager [14]. Multislice spin-echo acquisition was performed using a two-dimensional fourier transfer technique. Flow phantom experiments were performed using a standard double-saddle 30-cm head coil and also a 12-cm experimental animal coil. The acquisition matrix was 128 × 128 corresponding to 1.7-mm spatial resolution in the plane. The slice thickness was 7 mm. The repetition time (TR) of 500 msec was used for all experiments, with echoes acquired at echo-delay times (TE) of 28 and 56 msec.

A flow phantom was constructed of 1-cm-ID Tygon tubing looped within the bore of the magnet (fig. 6). The flow phantom was positioned in the center of the magnet, 1 m from the end of the bore. For simplicity, a stationary tube of water adjacent to the tubes containing flowing water. This allowed a direct comparison of flowing and stationary fluids without the necessity to consider different magnetic relaxation times or the potential effects of plasma-skimming during rapid blood flow [6]. Since pure water has a longer T1 than blood, it must remain within the magnetic field a longer period of time to become fully magnetized. The return loop has a course of 3 m within the bore of the magnet, which assures essentially full magnetization of water even at the highest flow rates used. Images from incoming and return limbs were compared in all experiments to assess potential effects of partial magnetization at high velocity.

Steady flow was achieved using a large gravity-feed tank, the flow rate being adjusted by varying the relative elevations of the influx and efflux lines. Entrance conditions were adjusted to allow full development of laminar flow within the phantom at low velocities. The course of the tubing 2 m upstream from the entrance to the magnet was aligned with the tubing within the magnet. Laminar flow was verified using dye-infusion experiments similar to those described below. Despite a gentle curvature over the 2-m return course, mild streaming was noted in the return loop (i.e., perfect laminar flow conditions were not maintained).

The volumetric flow rate was determined using timed flow into a graduated cylinder. MRI was performed using the Tygon-tubing flow phantom for volumetric flow rates (Q) of 10–750 ml/min.

A second flow phantom was constructed using 1.6-cm-ID Lucite tubing with a half-moon Lucite disk causing partial (63%) luminal obstruction. The appearance of flow in the vicinity of this obstruction was evaluated using dye-infusion experiments and MRI. The flow rate was set to about 50 ml/min, corresponding to a bulk Reynolds number of 650.

Food color was steadily infused through a port immediately downstream from the obstruction. Dye flow rate was under gravity field and adjusted to optimize demonstration of flow patterns. Overhead fluorescent lighting and a standard Canon *f*-1 35-mm camera fitted with a 70–210 mm Macro lens were used. High-speed (1000 ASA) film and rapid (1/500–1/1000) shutter speeds were used.

After the phantom experiments, clinical MR images were retro-

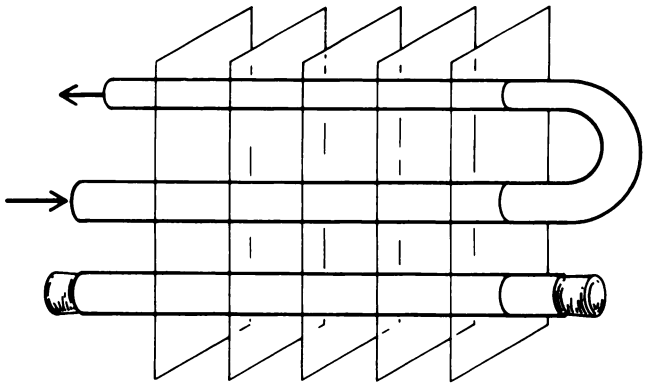

Fig. 6.—Flow phantom. Loop of 1-cm-ID Tygon tubing is positioned in center of magnet adjacent to similar tube filled with stagnant water.

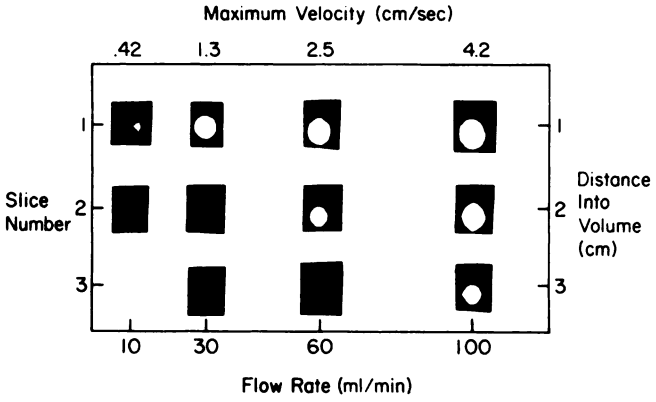

Fig. 7.—Signal intensities demonstrated as function of flow rate, calculated maximum velocity, and distance into volume. Highest intensity is seen on entry slice (numbered 1) with decreasing signal (and decreasing cross-sectional area) noted on slices greater distance into imaging volume. Intensity of signal from inner slices is greatest at higher flowrates. TR = 500 msec, TE = 28 msec.

spectively reviewed to obtain examples of the flow phenomena described.

Results

Experimental results from the Tygon-tubing flow phantom are shown in figure 7. The intraluminal MR signal is displayed graphically for flow rates of 10–100 ml/min in the first three slices encountered by the flowing water. Although the volumetric flow rate can be measured exactly, the linear velocity v at different radial positions across the diameter of the tube must be calculated. The average velocity is easily determined from the relation: $Q = v \times A$, where A is the cross-sectional area of the tube. For laminar flow, the maximum velocity in the center of the tube is twice the average velocity. Figure 7 demonstrates decreasing MR intensity on slices a greater distance into the imaging volume (i.e., further removed from the entry surface). At higher flow rates, greater-intensity MR signal is observed on slices further into the imaging volume.

Figure 8 displays the intraluminal signal in the transitional region between laminar and turbulent flow at flow rates of 200–750 ml/min. The first- and second-echo images are shown at the entry surface of a multislice imaging volume. In the laminar flow regime (Re = 800), increased signal intensity is noted on the second echo. As the Reynolds number is increased to 2000, the cross-sectional area of the first echo is seen to decrease, while the second-echo image loses intensity centrally and gains signal intensity peripherally. As the Reynolds number is increased further to 3000, the central hole on the second echo enlarges, decreasing the width of the peripheral band of increased intensity. At velocities of 20 and 30 cm/sec, the images were acquired from the return loop to allow the flowing water to become fully magnetized. Thus, even at a velocity of 30 cm/sec, the water has been within the magnetic field for 10 sec before reaching the return loop of the phantom 3 m from the entry surface. This corresponds to four T1 relaxation intervals, which allows recovery of 98% of the longitudinal magnetization [15]. Secondary streaming characteristics in the return loop can be seen in the second-echo images at higher velocity (fig. 8).

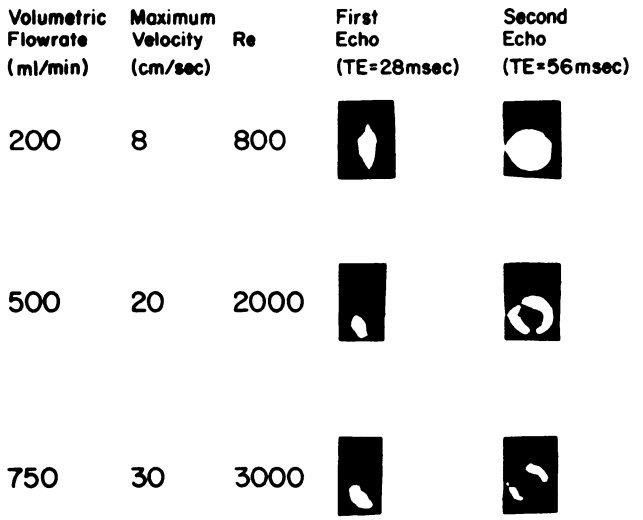

Fig. 8.—Intensity of rapidly flowing water. Flow phantom experiments demonstrate turbulent rephasing in buffer zone on second echo and greater high-velocity signal loss in central part. TR = 500 msec, Re = Reynolds number.

Figure 9 demonstrates the flow pattern from a dye-infusion experiment using the Lucite flow phantom. Here a large-scale recirculation zone is noted downstream from the obstruction, and small wavelike formations are noted, indicating transition to turbulent flow through the orifice. The MRI appearance through the lumen 1 cm downstream from the obstruction is shown in figure 10. Increased signal intensity is noted on the second echo in the lower half of the lumen where the eddy is seen on the corresponding dye-infusion image.

Figure 11 demonstrates the first five slices of a 15-slice non-cardiac-gated imaging sequence through the neck of a normal volunteer with a heart rate of 80. The slices are numbered as they are encountered by blood flowing in the carotid artery. The area of the intraluminal signal within the

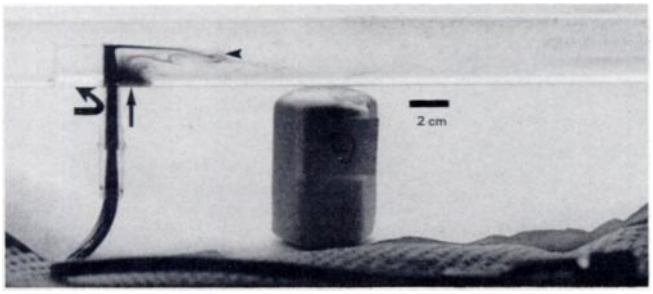

Fig. 9.—Dye-infusion pattern. Flow within Lucite tube is from reader's left to right, past Lucite disk (*curved arrow*), causing 63% obstruction. Dye is infused immediately downstream from this obstruction leading to large scale recirculation zone in corner (*arrow*) with early wavelike formations (*arrowheads*), indicating transition to turbulence in rapid flow through orifice.

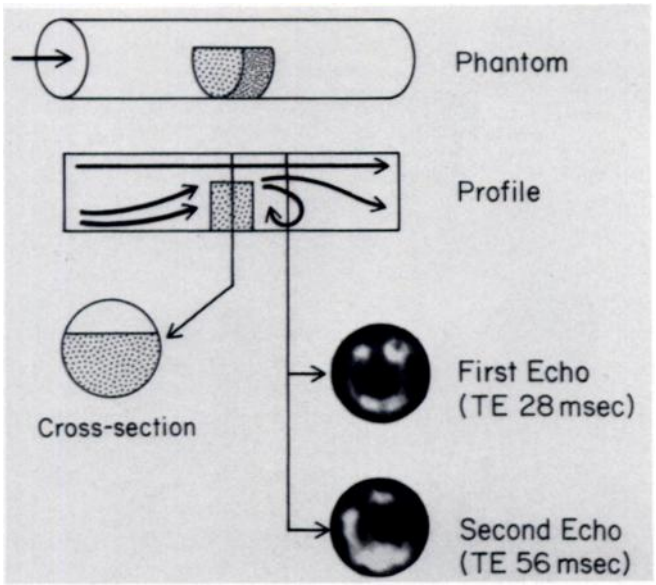

Fig. 10.—Even-echo rephasing downstream from obstruction in turbulent flow. Lucite phantom is shown schematically, as are flow patterns in lateral projection. Actual axial MR images 1 cm downstream from obstruction are shown, demonstrating even echo rephasing in eddy. TR = 500 msec.

carotid artery is seen to decrease for slices a greater distance into the imaging volume. A patient with a 6-cm infrarenal aortic aneurysm is shown in figure 12. Increased signal intensity is noted on the second-echo image along the left lateral aspect of the patent lumen adjacent to the mural thrombus.

Discussion

The strong signal intensity noted at the entry surface of a multislice imaging volume during laminar flow (fig. 7) represents flow-related enhancement [9]. This is due to unsaturated protons initially entering the imaging volume with full magnetization compared with the partially saturated protons in the adjacent fluid, which have not yet fully recovered from

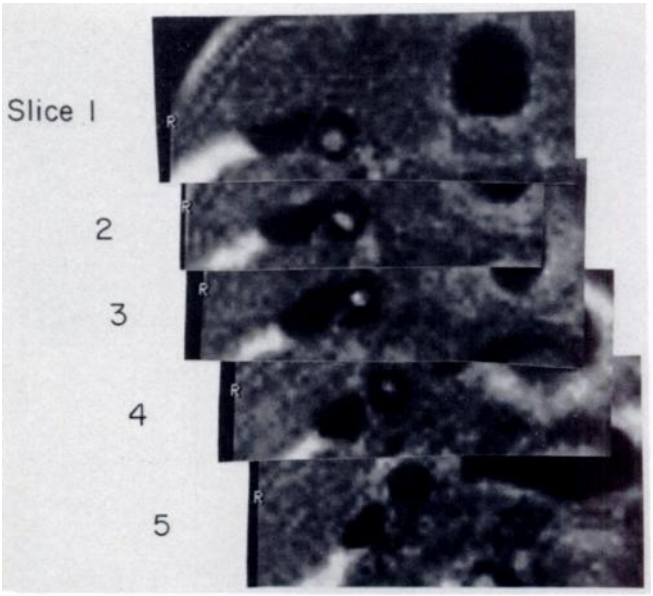

Fig. 11.—Multislice flow-related enchancement in right common carotid artery. TR = 1500 msec, TE = 28 msec, nongated. Decreasing intraluminal signal is noted for slices greater distance into imaging volume. (Slice 1 is entry slice.) This reflects flow of unsaturated protons several slices into imaging volume (demonstrated schematically in fig. 14).

the previous excitation (fig. 13). This has been described previously for the first slice encountered by blood flowing into a multisclice imaging volume [4, 8, 9]. Although decreasing intraluminal signal has been noted previously as a function of distance into the imaging volume [8], this has not been related to flow rate nor has a signal with decreasing cross-sectional area been demonstrated on slices deeper into the imaging volume. This phenomenon can be explained by considering the volume of unsaturated protons that enter the imaging volume during the period between excitations (fig. 14). During laminar flow, the flow profile is parabolic; thus, slices deeper into the imaging volume will demonstrate decreasing cross-sectional area of the intense central signal, which represents the unsaturated protons.

At higher velocities, several competing effects determine the appearance of flowing fluid (fig. 8). In the laminar flow regime (Re = 800), increased signal from the second echo is present due to even-echo rephasing [7]. As the flow rate is increased to 500 ml/min and turbulence starts to appear (Re = 2000), signal is lost from the buffer zone between the core and the peripheral laminar sublayer. This is the zone of greatest random motion, which therefore causes the greatest loss of coherence and subsequent loss of spin-echo signal intensity. Signal is maintained in the turbulent core, where the intensity of random motion is actually less than in the buffer zone [10]. On the second echo at this flow rate, signal is lost from the center due to high velocity. Protons in the center of the tube that were within the selected slice for the period between the 90° pulse and the *first* 180° pulse (14 msec) have flowed out of the slice during the longer interval between 90° pulse and the *second* 180° pulse (42 msec). Increased signal is noted on the second-echo image in the buffer zone

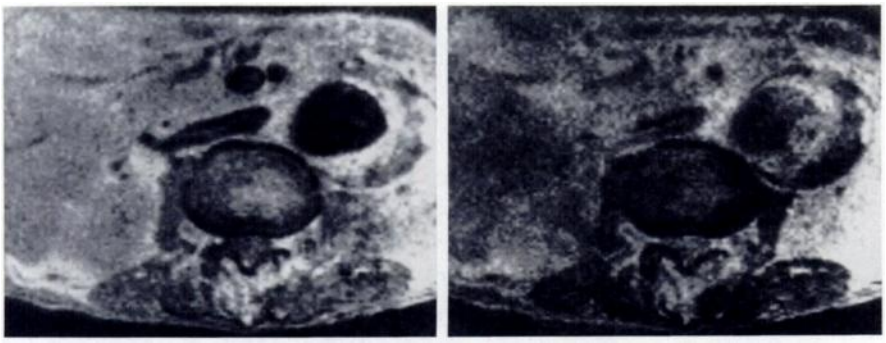

Fig. 12.—Infrarenal aortic aneurysm. **A,** TR = 2000 msec, TE = 28 msec. Mural thrombus is noted eccentrically along left lateral aspect of aneurysm in transaxial image through abdomen. **B,** TR = 2000 msec, TE = 56 msec. Second-echo image demonstrates increased signal between thrombus and more rapid flow along right lateral border of aneurysm. Because such signal is not present on first echo, it cannot be solid and must therefore represent rephasing phenomenon. Note also rephasing and increased second-echo intensity in inferior vena cava and superior mesenteric artery and vein.

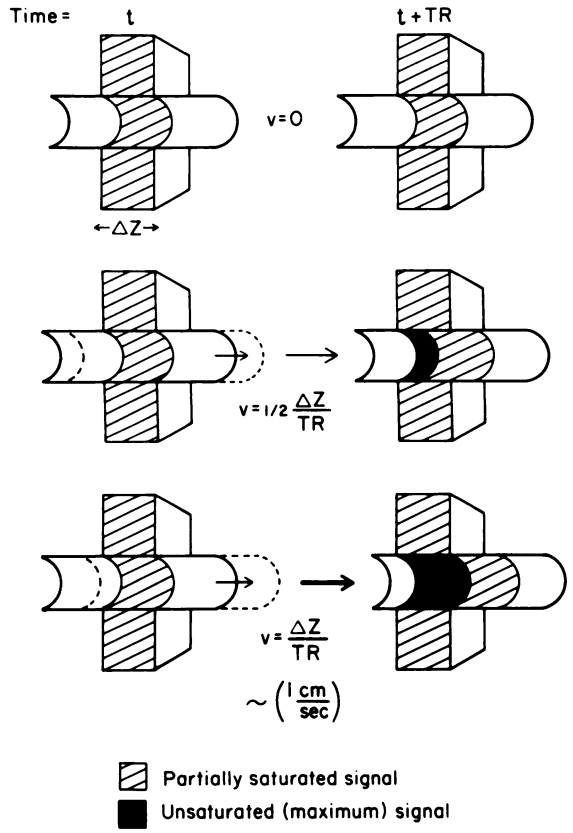

Fig. 13.—Flow-related enhancement. Unsaturated protons enter first slice of imaging volume with full magnetization and thus give stronger signal than partially saturated protons in adjacent stationary tissue. Maximal flow-related enhancement occurs at velocity v, such that distance equal to slice thickness Δz is traversed during repetition time TR.

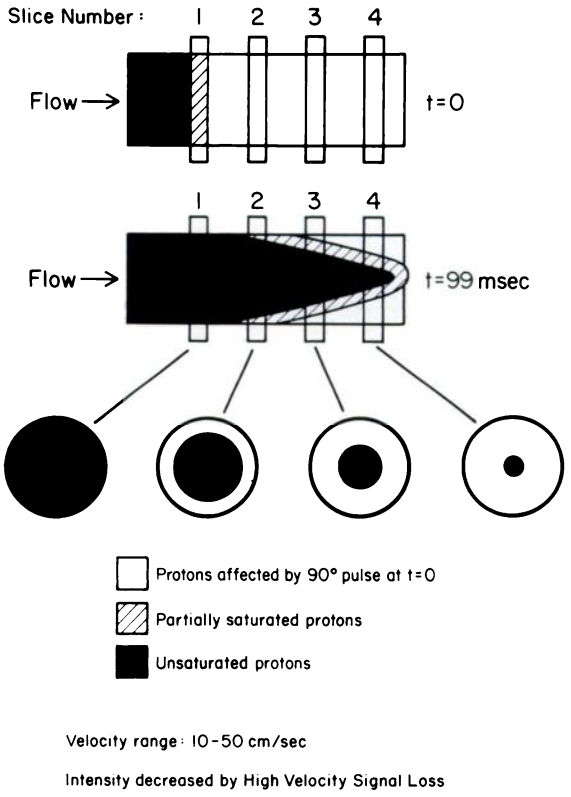

Fig. 14.—Multislice flow-related enhancement. When laminar flow is maintained at higher velocities, parabolic laminar profile can project several slices into imaging volume. In order for unsaturated protons to be present centrally, they must traverse distance from entry surface to specific slice during time between 90° pulses (i.e., 100 msec). Cross-sections of laminar profile result in decreasing cross-sectional area for central zone of unsaturated protons deeper into imaging volume. t = time.

surrounding the central region of signal loss. Since there was no signal on the first-echo image, this must represent a rephasing phenomena. At a Reynolds number of about 2000, one would expect turbulence in this buffer zone; thus, figure 8 shows turbulent rephasing. As the flow rate is increased to 750 ml/min, the size of the hole on the second echo increases due to increased high-velocity signal loss at the higher flow rate. The rim of increased intensity persists but is thinned and again represents turbulent rephasing in the buffer zone. This is demonstrated schematically in figure 15.

Turbulence can be caused by high-velocity flow within a smooth tube or it can be caused by irregularities in the wall of the tube, including partial intraluminal obstructions [10, 11]. Figures 9 and 10 demonstrate flow past a 63% obstruction and illustrate two phenomena associated with turbulence. Even-echo rephasing is demonstrated in the large-scale recirculation zone downstream from the obstruction. Laminar flow is present within this eddy, which results in increased signal

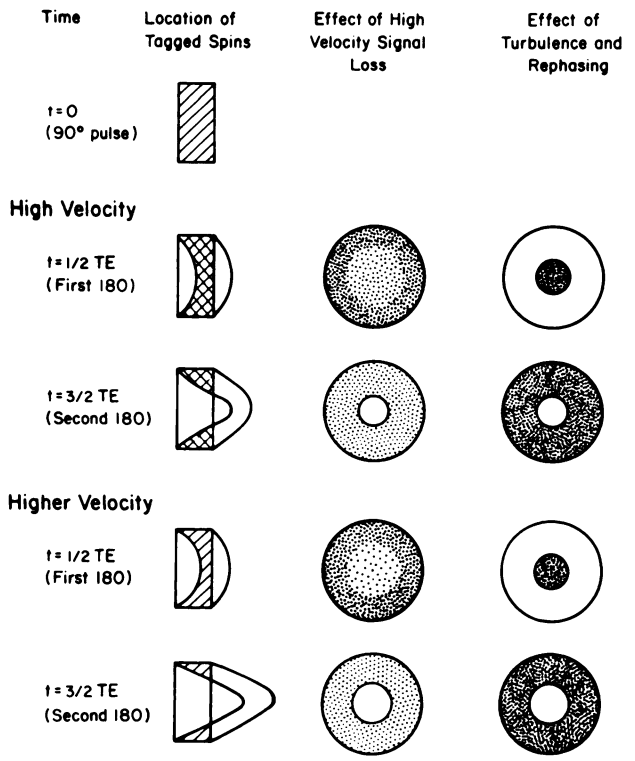

Fig. 15.—Intensity of rapidly flowing blood. Since both 90° and 180° pulse must be acquired to generate spin-echo signal, protons exposed to both pulses are demonstrated with cross-hatching in lateral projection (*left column*). Subpopulation of those protons receiving initial 90° pulse has moved out of slice in early parabolic profile at time of first 180° pulse (t = ½TE) and into steeper parabolic profile at time of second 180° pulse (t = ⅔TE). Pattern is more pronounced at higher velocity. Seen en face (*middle and right columns*), this causes central decreased intensity in first echo with higher intensity noted in more slowly flowing periphery. By time of second 180° pulse, which results in second-echo image, central protons have actually left slice, leading to total absence of signal. Size of central hole is increased at higher velocity. Effect of turbulence is to decrease signal in buffer zone due to increasing random motion and loss of coherence. Signal is maintained on first echo in central core where magnitude of random motion is less than in buffer zone. Rephasing occurs on second echo in buffer zone, giving "donut" appearance. (Rephasing cannot overcome effects of high velocity signal loss; thus, central hole remains.)

intensity on the second echo relative to the first. In addition, turbulence is present at the orifice. The turbulence decreases the signal at the orifice, both from increased random motion and from high-velocity signal loss. The latter is apparently dominant at the particular flow rate used, since there is no rephasing on the second echo in the upper half of the image through the region 1 cm downstream from the orifice.

Figures 11 and 12 demonstrate potential clinical applications of the phenomena demonstrated in the flow phantom experiments. Intraluminal signal on MRI can potentially be mistaken for thrombus or tumor and, thus, other causes of increased intraluminal signal must be excluded. Figure 11 demonstrates that flow-related enhancement can in fact extend several slices into a multislice imaging volume if the flow rate is high enough and laminar flow is maintained. A pattern of decreasing signal area for slices deeper into the imaging volume would suggest this phenomenon rather than true pathology. It is interesting that this pattern, which is predicted for steady laminar flow, is observed regularly on nongated images in the common carotid arteries. Laminar flow in the common carotid artery is expected during parts of the cardiac cycle [16]. Although pulsatile flow totally out of phase with the MR acquisition sequence should show no pattern, "pseudogating" [9] may be present in this patient with a heart rate of 80 when using a 1500-msec-TR pulsing sequence. (Pseudogating results when the TR and the heart rate are in phase, so that a given slice in a multislice imaging sequence is acquired at a given point in the cardiac cycle.)

Figure 12 demonstrates increased signal intensity on the nongated second-echo image within a patent aortic lumen. Since this signal is not present on the first echo, it must represent a rephasing phenomenon associated with turbulent flow in the aorta. From the eccentric appearance of the mural thrombus, flow is clearly more rapid along the right lateral and central part of the aneurysm; thus, high-velocity signal loss is noted on the second echo in this region.

Although water phantom experiments are useful to evaluate flow phenomena in an MR imager, they obviously represent an approximation of the true in vivo situation. Both blood and adjacent tissue have shorter T1 and T2 values than water. Thus, the absolute intensities of the phenomena described above will differ from those shown here, although the behavior will be similar. Blood flow in arteries such as the aorta is pulsatile and may be associated with significant backflow during diastole [11]. Because blood has a higher viscosity than water, higher velocities are tolerated before turbulence occurs. The phenomena illustrated here are for flow perpendicular to the imaging planes; oblique or in-plane flow will exhibit somewhat different characteristics. Finally, the actual appearance of flowing blood will be modified by the specific pulsing sequences used on a given imager and by different gradient fields on different imagers. Thus, as complicated as water phantoms are, they may still incompletely describe the true clinical appearance of rapidly flowing blood.

In summary, several new rapid-flow phenomena observed clinically on MRI have been studies using phantoms. Flow-related enhancement has been shown to involve several slices near the entry surface of a multislice imaging volume. Decreasing cross-sectional area of the intense center is noted on slices a greater distance into the volume. At higher velocities, where turbulence is expected, rephasing is noted within the buffer zone on the second-echo image, while there is central loss of signal due to increased high-velocity signal loss. Such phenomena may be observed clinically, especially in large-diameter vessels, which are more prone to develop turbulence. Flow through an obstruction has also been evaluated, demonstrating even-echo rephasing in the large-scale recirculation zone downstream from the obstruction. Since such zones can extend far beyond the obstruction, even-echo rephasing in this region may be a sensitive indicator of a hemodynamically significant obstruction upstream.

ACKNOWLEDGMENT

We thank Kaye Finley for manuscript preparation and Jay Mericle, Terry Andrues, and Leslee Watson for technical assistance.

REFERENCES

1. Hawkes RC, Holland GN, Moore WS, Worthington BS. Nuclear magnetic resonance (NMR) tomography of the brain: a preliminary clinical assessment with demonstration of pathology. *J Comput Assist Tomogr* **1980**;4:577–586
2. Young IR, Burl M, Clarke GJ, et al. Magnetic resonance properties of hydrogen: imaging in the posterior fossa. *AJR* **1981**;137:895–901
3. Gore JC. The meaning and significance of relaxation in NMR imaging. In: Witcofski RL, Karstaedt N, Partain CL, eds. *Proceedings of the NMR symposium.* Winston-Salem, NC: Bowman-Gray School of Medicine Press, **1981**:15–24
4. Crooks LE, Mills CM, Davis PL, Brant-Zawadzki M, et al. Visualization of cerebral and vascular abnormalities by NMR imaging: the effects of imaging parameters on contrast. *Radiology* **1982**;144:843–852
5. Kaufman L, Crooks L, Sheldon P, Hricak H, Herfkens R, Bank W. The MR signal intensity patterns obtained from continuous and pulsatile flow models. *Radiology* **1984**;151:421–428
6. George CR, Jacobs G, MacIntyre WJ, Lorig RJ, Go RT, Nose T, Meaney TF. MR signal intensity patterns obtained from continuous and pulsatile flow models. *Radiology* **1984**;151:421–428
7. Waluch V, Bradley WG. NMR even echo rephasing in slow laminar flow. *J Comput Assist Tomogr* **1984**;8:594–598
8. Mills CM, Brant-Zawadzki M, Crooks LE, et al. Nuclear magnetic resonance: principles of blood flow imaging. *AJNR* **1983**;4:1161–1166
9. Bradley WG, Waluch V. Magnetic resonance imaging of blood flow. *Radiology* (in press)
10. Bird RB, Stewart WE, Lightfoot EN. *Transport phenomena.* New York: Wiley, **1960**:153–158
11. McDonald DA. Blood flow in arteries. Baltimore: Williams & Wilkins, **1960**:20
12. DeGennes PG. Theory of spin echoes in a turbulent field. *Phys Letters* **1969**;29A:20–21
13. Deville G, Landesman A. Experiences d'echos de spins dans un liquide en ecoulement. *J Physique* **1971**;32:67–72
14. Crooks LE, Arakawa M, Hoenninger JC, et al. NMR whole body imager operating at 3.5 kgauss. *Radiology* **1982**;143:169–174
15. Bradley WG, Crooks LE, Newton TH. Physical properties of NMR. In: Newton TH, Potts DG, eds. *Advanced imaging techniques*, vol 2, chap 3. San Francisco, Calvadel, **1983**
16. Motomiya M, Karino T. Flow patterns in the human carotid artery bifurcation. *Stroke* **1984**;15:50–56